Radio Science, Volume 19, Number 4, Pages 1083–1097, July–August 1984

Maps of $f_o F_2$ derived from observations and theoretical data

Charles M. Rush,[1] *Margo PoKempner,*[2] *David N. Anderson,*[3] *Jane Perry,*[4] *Frank G. Stewart,*[1] *and Rita Reasoner*[1]

(Received January 19, 1984; revised March 28, 1984; accepted March 28, 1984.)

Observations of the F_2 region critical frequency, $f_o F_2$, and values determined from the time-dependent continuity equation for ions and electrons in the ionosphere have been used to develop a new set of numerical coefficients to represent the global variation of $f_o F_2$. Like those in earlier investigations, the new coefficients permit monthly median hourly values of $f_o F_2$ to be obtained at any location around the globe for any month of the year and solar activity level. Comparisons between $f_o F_2$ determined using older sets of numerical coefficients and $f_o F_2$ determined using the new set of coefficients are given along with a description of how well each set of coefficients specifies and predicts the observed variations in the F_2 region critical frequency.

1. INTRODUCTION

The structure of the F_2 region varies with time and space and imparts associated variations upon the radio signals that traverse it. The critical frequency of the F_2 region, $f_o F_2$, is a fundamental parameter that is used in the specification and prediction of the structure of the F_2 region. Global maps of $f_o F_2$ derived from numerical coefficients are used as the basis for various ionospheric models [*Nisbet*, 1971], HF propagation prediction methods [*Lucas and Haydon*, 1966; *Nielson et al.*, 1967; *Barghausen et al.*, 1969; *Haydon et al.*, 1976; *CCIR*, 1982*a*; *Teters et al.*, 1983], and transionospheric propagation models [*Bent et al.*, 1978]. The numerical coefficients were developed at the Institute for Telecommunication Sciences by using the procedure described by *Jones and Gallet* [1962]. They have been accepted by the International Radio Consultative Committee (CCIR) and are used in the HF propagation prediction programs produced by that body. Because they are available from the CCIR, they are referred to in the text as the CCIR maps.

The accuracy of the global representation of $f_o F_2$ obtained from the CCIR maps is dependent upon the geographical distribution of the stations whose data were used in the generation of the numerical coefficients. Where observations were available for inclusion in the analysis that generated the coefficients, the accuracy of $f_o F_2$ is quite reasonable [*King and Slater*, 1973]. At locations where data were not available (such as oceans), the accuracy of $f_o F_2$ determined from the coefficients is questionable.

In a recent paper, *Rush et al.* [1983] described how theoretically derived values of $f_o F_2$ could be used to improve the global representation of $f_o F_2$ that is produced by using the CCIR numerical coefficients [*CCIR*, 1982*b*]. The improvement is obtained by combining values of $f_o F_2$ derived from the time-dependent continuity equation for ions (and electrons) with monthly median observations of $f_o F_2$ to obtain expanded data bases that can be subjected to spherical harmonic analysis. The harmonic analysis then yields coefficients that represent a global variation of $f_o F_2$ that is consistent with both observations and the current understanding of the physical mechanisms responsible for the large-scale ionospheric variations.

The results presented by *Rush et al.* [1983] were confined to the months of July, September, and December and the years 1975 and 1978. The results for the year 1975 were taken as being indicative of sunspot minimum conditions and those for 1978 were indicative of sunspot maximum conditions. A limited number of comparisons between $f_o F_2$ values derived from the CCIR maps and the $f_o F_2$ values derived from the new coefficients were also given. Since that paper was published, numerical coefficients for each month of a sunspot minimum and a sunspot maxi-

[1] Institute for Telecommunication Sciences, National Telecommunications and Information Administration, U.S. Department of Commerce.

[2] Contractor to Institute for Telecommunication Sciences.

[3] Air Force Geophysics Laboratory.

[4] Department of Defense, Washington, D. C.

Paper number 4S0506.

mum year have been developed that are based upon the same principles as given by *Rush et al.* [1982, 1983]. It is the purpose of this paper to describe the most recent results obtained and to present detailed comparisons of observed f_oF_2 values with values of f_oF_2 derived from the CCIR maps and with values of f_oF_2 derived from the new coefficients.

2. DATA AND DATA SOURCES

In developing the first set of numerical maps of ionospheric data, *Jones and Gallet* [1962] found it necessary to ensure that f_oF_2 data existed at sufficient locations so that the mapped fields did not have negative values. These negative values resulted from instabilities in the maps in areas where data were either nonexistent or sparse. In order to prevent instabilities, Jones and Gallet employed a "screen analysis" whereby observations available at specific locations were extrapolated to areas devoid of data taking account of the geomagnetic field control of the F_2 region [*Jones and Gallet*, 1965]. Inherent in this procedure is the assumption that the temporal variations in f_oF_2 at one location (observation point) are related to those at another location (extrapolated point) in a relatively simple manner. However, the inaccuracies in the maps over the ocean areas, for example, point up the need for better estimates of the behavior of f_oF_2 in regions of the earth that are inaccessible to routine observations.

In the development of the new set of numerical coefficients discussed in this paper, the screen analysis of *Jones and Gallet* [1965] was abandoned in favor of a more physically based approach. In order to obtain a uniform data set that could be subjected to the spherical harmonic analysis techniques used by Jones and Gallet, observations of f_oF_2 obtained from vertical-incidence ionosondes were combined with f_oF_2 values determined from the time-dependent continuity equation for ions (and electrons).

Numerical coefficients that represent the global variations of f_oF_2 have been determined for each month for July 1975 to June 1976 and for July 1978 to June 1979. The coefficients for July 1975 to June 1976 are representative of solar minimum conditions and those for July 1978 to June 1979 are representative of solar maximum conditions. Table 1 lists the 12-month average Zurich sunspot number for each of the months for which coefficients were derived. It is evident from the table that for solar minimum (1975/1976), the sunspot numbers do not vary greatly from month to month and are typically of the order of 10–15 units. For solar maximum (1978/1979), however, the sunspot number increases continuously from 95 in July 1978 to 154 in June 1979. Thus the coefficients obtained in this study for solar maximum may not accurately represent the highest solar maximum conditions that are observed, particularly for the months July through December 1978.

Monthly median observations of f_oF_2 obtained from the stations given in Table 2 form the basis for the spherical harmonic analysis. In the table, the station name and location in geographic coordinates are given. Also given in the table is the letter A or B under each of the two solar cycle epochs. The letter A refers to data that were observed at the station for the time period 1975/1976 and/or 1978/1979. The letter B refers to data observed at the station in question for a different solar epoch and adjusted to the solar epochs in 1975/1976 or 1978/1979 using a polynomial interpolation procedure [*Crow and Zacharisen*, 1960]. To obtain values of f_oF_2 from the interpolation procedure for a given location, observations at that location had to be available for the month in question for other solar epochs. Data of this type are referred to in this paper as B data. The use of data similar to B data in other geophysical disciplines has been pointed out by *Rush et al.* [1982]. Actual observed monthly median data are denoted as A data.

Figure 1 depicts the distribution of A and B data sources throughout the world. The figure vividly illustrates the lack of uniformity in the distribution of

TABLE 1. Smoothed Observed Sunspot Numbers for July 1975 Through June 1976 and July 1978 Through June 1979

	Jan.	Feb.	March	April	May	June	July	Aug.	Sept.	Oct.	Nov.	Dec.
1975							15.0	14.3	14.5	15.6	16.3	16.5
1976	15.2	13.2	12.2	12.6	12.5	12.2						
1978							95.0	104.0	108.4	111.0	113.3	116.7
1979	122.8	130.4	136.1	141.0	147.3	153.7						

TABLE 2. Ionosonde Stations Providing Data Used in the Determination of $f_0 F_2$ Coefficients

Station Name	Latitude, °N	Longitude, °E	1975/1976	1978/1979
Arctic I (USSR) Floating Ice Island			B	B
Arctic II (USSR) Floating Ice Island			B	B
Arctic III (USSR) Floating Ice Island			B	B
Heiss Island, USSR	80.6	58.0	A	B
Thule, Greenland	76.4	291.3	B	B
Resolute Bay, Canada	74.7	265.1	A	A
Dixon Island, USSR	73.5	80.4	B	B
Barrow, Alaska	71.3	203.2	B	B
Godhavn, Greenland	69.3	306.5	B	B
Kiruna, Sweden	67.8	20.4	A	A
Sodankyla, Finland	67.4	26.6	A	A
Salekhard, USSR	66.5	66.7	A	A
Lycksele, Sweden	64.7	18.8	A	A
Archangelsk, USSR	64.6	40.5	—	A
Providenya, USSR	64.4	186.6	B	B
Tunguska, USSR	61.6	90.0	—	A
Yakutsk, USSR	62.0	129.6	—	A
Narssarssuaq, Greenland	61.2	314.6	B	B
Anchorage, Alaska	61.2	210.1	B	B
Leningrad, USSR	60.0	30.7	A	A
Nurmijarvi, Finland	60.5	24.6	A	A
Uppsala, Sweden	59.8	17.6	A	A
Churchill, Canada	58.8	265.8	A	A
Gorky, USSR	56.1	44.3	A	A
Sverdlovsk, USSR	56.7	61.1	A	A
Tomsk, USSR	56.5	84.9	A	A
Juliusruh/Rugen, Federal Republic of Germany	54.6	13.4	A	A
Moscow, USSR	55.5	37.3	A	A
Goosebay, Canada	53.3	299.2	A	A
De Bilt, Netherlands	52.1	5.2	A	A
Pruhonice, Czechoslovakia	50.0	14.6	A	A
Miedzeszyn, Poland	52.2	21.2	A	A
Irkutsk, USSR	52.5	104.0	A	A
Slough, England	51.5	359.4	A	A
Adak, Alaska	51.9	183.4	B	B
Lindau, Federal Republic of Germany	51.6	10.1	A	A
Dourbes, Belgium	50.1	4.6	A	A
Rostov, USSR	47.2	39.7	A	A
Winnipeg, Canada	49.8	265.6	A	—
Freiburg, Federal Republic of Germany	48.1	7.6	A	—
Khabarovsk, USSR	48.5	135.1	A	A
Lannion, France	48.5	356.7	A	A
Budapest, Hungary	46.7	21.2	A	—
Saint John's, Canada	47.6	307.3	A	—
Poitiers, France	46.6	0.3	A	A
Wakkanai, Japan	45.4	141.7	A	A
Ottawa, Canada	45.4	284.1	A	A
Alma-Ata, USSR	43.2	76.9	A	A
Tbilisi, USSR	41.7	44.8	A	A
Rome, Italy	41.8	12.5	A	B
Tashkent, USSR	41.3	69.6	—	A
Tortosa, Spain	40.8	0.3	A	B
Boulder, Colorado	40.0	254.7	A	A
Akita, Japan	39.7	140.1	A	A
Gibilmanna, Sicily	38.0	14.0	—	A
Ashkabad, USSR	37.9	58.3	A	A
Seoul, South Korea	37.4	127.0	A	A
Wallops, Virginia	37.9	284.5	A	A
Point Arguello, California	35.6	239.4	A	A
Tokyo, Japan	35.7	139.5	A	A
White Sands, New Mexico	32.3	253.5	—	A
Yamagawa, Japan	31.2	130.6	A	A
Wuhan, China	30.6	114.4	A	A
Delhi, India	28.6	77.2	B	B
Okinawa, Japan	26.3	127.8	A	A
Taipei, Taiwan	25.0	121.2	A	A
Ahmedabad, India	23.0	72.6	B	B
Hong Kong, Southeast Asia	22.3	114.2	B	B
Maui, Hawaii	20.8	203.5	A	A
Mexico City, Mexico	19.4	260.3	A	A
Dakar, Senegal	14.7	342.6	A	B
Manila, Philipine Islands	14.7	121.1	A	A
Bangkok, Thailand	13.7	100.6	A	A
Ouagadougou, Upper Volta	12.4	358.5	A	A
Djibouti, Northeast Africa	11.6	42.8	A	A
Kodaikanal, India	10.2	77.5	A	—
Thumba, India	8.6	76.9	A	—
Vanimo, New Guinea	−2.7	141.3	A	A
Huancayo, Peru	−12.0	284.7	A	A
Tahiti, Pacific Ocean	−17.7	210.7	A	A
Tsumeb, Namibia	−19.2	17.7	A	—
Townsville, Australia	−19.3	146.7	A	A
Raratonga, Cook Island	−21.2	200.2	A	A
Johannesburg, South Africa	−26.1	28.1	A	A
Tucuman, Argentina	−26.9	294.6	A	A
Brisbane, Australia	−27.5	152.9	A	A
Norfolk Island, Pacific Ocean	−29.0	168.0	A	A
Mundaring, Australia	−32.0	116.2	A	A
Capetown, South Africa	−34.1	18.3	A	—
Buenos Aires, Argentina	−34.5	301.5	A	—
Canberra, Australia	−35.3	149.0	A	A
Concepcion, Chile	−36.6	287.0	A	A
Auckland, New Zealand	−37.0	175.0	A	A
Hobart, Australia	−42.9	147.2	A	A
Christchurch, New Zealand	−43.6	172.8	A	A
Kerguelen, Indian Ocean	−49.4	70.3	A	A
Port Stanley, Falkland Islands	−51.7	302.2	A	A
Campbell Island, Pacific Ocean	−52.5	169.2	A	A
South Georgia, Atlantic Ocean	−54.3	323.5	A	—
Argentine Island, Antarctica	−65.2	295.7	A	A
Casey Base, Antarctica	−66.2	110.5	B	B
Mirny, Antarctica	−66.5	93.0	B	B

TABLE 2. (continued)

Station Name	Latitude, °N	Longitude, °E	1975/ 1976	1978/ 1979
Terre Adelie, Antarctica	−66.7	140.0	A	A
Mawson, Antarctica	−67.6	62.9	B	A
Syowa Base, Antarctica	−69.0	39.6	A	A
Sanae, Antarctica	−70.3	357.6	A	A
Halley Bay, Antarctica	−75.5	333.4	A	A
Scott Base, Antarctica	−77.8	166.8	A	A
Vostok, Antarctica	−78.4	106.9	B	B
Byrd Station, Antarctica	−80.0	240.0	B	B
South Pole, Antarctica	−90.0	0.0	B	B

The symbol A indicates that median observations for the time period in question were used in the analysis. The symbol B indicates that observations were used to predict the median value of f_oF_2 for the time period in question.

observed data throughout the globe. Obviously A and B data sources are available over land-based regions. Most of the globe, however, is not covered with these observations. It is this situation that was ameliorated by using the time-dependent continuity equation to generate f_oF_2 values in the data-sparse areas. In actual fact, the continuity equation was used to determine f_oF_2 values only at middle and high latitudes (latitudes greater than about 25° north or south magnetic latitude).

The data needed for the unobserved regions in the equatorial ionosphere were not derived in as rigorous a fashion as those for the unobserved regions at other latitudes. This is due primarily to the fact that for the time-dependent continuity equation to yield realistic values of f_oF_2 at low magnetic latitudes, the vertical electrodynamic drift at the equator must be included in the calculation. This results in calculations that are very lengthy and time-consuming even for modern computers. It was determined that it was impractical in this investigation to obtain values of f_oF_2 needed for the low latitudes from the theoretical or time-dependent continuity equation. Rather, what was done was to take f_oF_2 observations at the available low-latitude locations and plot them onto global maps for each hour of local time. The variation of f_oF_2 plotted at constant local time was found to be much smoother than when it was plotted in constant universal time. Contours of constant f_oF_2 were then constructed at each hour of local time for each month from the plotted values of f_oF_2. It was found that distinct and noticeable differences in the shape and form of the contours had to be drawn for regions of the globe where the magnetic field has an eastward declination and where it has a westward declination. Once the contours were drawn for each hour of local time for a given month, the local time maps were used to determine f_oF_2 at specific points in the low-latitude ionosphere. These low-latitude values were then combined with the values of f_oF_2 determined from the time-dependent continuity equations and the A and B data to provide the data base needed to generate numerical coefficients from the spherical harmonic analysis of *Jones and Gallet* [1962].

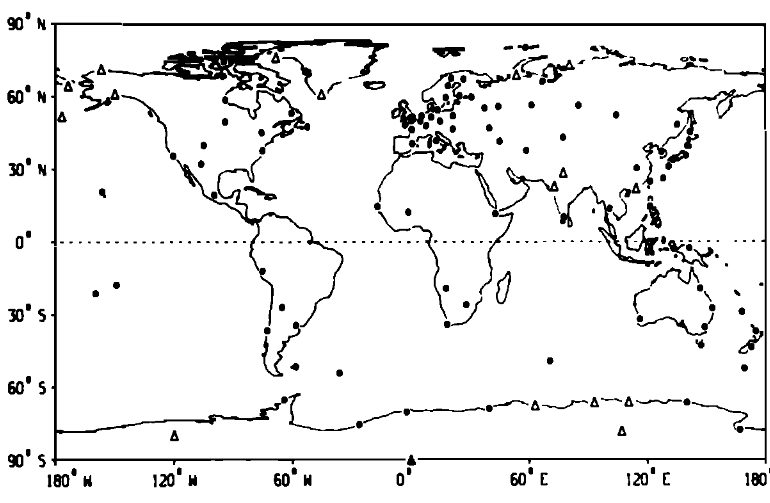

Fig. 1. Location of ionosonde stations providing data used in determination of f_oF_2 coefficients. The open triangles refer to those locations where B data were used for both solar epochs. The closed circles indicate the locations where A data were used for at least one of the two solar epochs.

3. THEORETICALLY DERIVED DATA

The time-dependent ion continuity equation was used to calculate values of f_oF_2 at middle and high latitude regions where observations of f_oF_2 were not available. The values were obtained by use of the technique as described by *Anderson* [1973] and applied to ionospheric mapping studies by *Rush et al.* [1983]. The values of f_oF_2 thus determined are referred to hereafter as theoretical values.

The time-dependent continuity equation is given by

$$\frac{\partial N_i}{\partial t} + \nabla \cdot (N\bar{V}_i) = P_i - L_i \tag{1}$$

where N_i is the ion density, P_i is the ion production rate, L_i is the loss rate, and $\bar{V}_i$ is the transport velocity. In the ionosphere, plasma is transported along the geomagnetic field lines by diffusion and neutral winds, and perpendicular to the field lines primarily by electrodynamic ($\bar{\mathbf{E}} \times \bar{\mathbf{B}}$) drifts. For the purposes of this investigation, it was assumed that at middle and high latitudes the transport of plasma along the field lines greatly exceeded the transport across the field lines [*Benkhe and Kohl*, 1974]. The movement of plasma due to electrodynamic drift was therefore neglected permitting a much simpler and computationally efficient solution to equation (1).

The continuity equation was solved numerically following *Anderson* [1973], to give N_i ($= N_e$, electron density) as a function of altitude, latitude, and local time. In arriving at a solution for N_i, it was assumed that the only ion of concern was atomic oxygen (O^+), a valid approximation for F_2 region heights. The parameters needed to solve the ion continuity equation were obtained from models of the neutral composition and temperature, ion and electron temperatures, production, loss and diffusion rates, and neutral wind. These models were determined for the appropriate month and sunspot number given in Table 1. The geomagnetic field model needed in order to arrive at a solution to equation (1) follows that given in *Anderson* [1973]. The models of the parameters used in the solution to the continuity equation are the same as those given by *Rush et al.* [1983] expanded to be valid for the entire time periods covered in this investigation.

The neutral wind models needed in the solution of the continuity equation were also determined by the methods described in *Rush et al.* [1983]. Meridional and zonal neutral wind models were determined for each of the months in the 1975/1976 and 1978/1979 time periods. Different models for the same months were obtained for the northern and southern hemispheres of the globe, and the winds were assumed to be independent of altitude.

Figure 2 provides examples of the neutral wind models for the months of March 1976 and 1979 for both the northern and southern hemispheres. The variations seen in the zonal and meridional winds in Figure 2 are typical of the neutral wind patterns observed for all the months used in this analysis. The zonal wind is directed eastward during the evening hours and, for some months, in the hours immediately following midnight. During solar maximum, the eastward zonal wind prevails in the winter hemisphere around the sunrise hours. This is not the case at solar minimum when the zonal wind is either absent or directed to the west during the sunrise hours. The meridional wind is directed equatorward during the night and early morning hours and is either absent or directed toward the poles during the daylight hours. Models for the neutral winds, as well as all the parameters for each month that were used in this study, are given by *Rush et al.* [1984].

The importance of including the effects of neutral winds in the solution to the continuity equation is that in the F region the neutral wind moves ionization along geomagnetic field lines. The equatorward meridional wind moves ionization up in altitude, and the poleward meridional wind moves ionization downward. The zonal wind imparts an upward or downward drift to the ionization depending upon the relative direction between the wind velocity and the declination of the geomagnetic field. In the southern hemisphere where the inclination of the geomagnetic field is directed upward, an eastward wind will impart a downward component to the ionization when the field is declined westward and an upward component when it is declined eastward. A westward wind in the southern hemisphere gives rise to an upward component when declination is westward and a downward component when the declination is eastward. The effect in the northern hemisphere is just the opposite because the inclination of the magnetic field lines is directed downward. Figure 3 provides a simplified illustration of the movement of ionization along the geomagnetic field due to zonal winds in the southern hemisphere and northern hemisphere for east and west geomagnetic declinations.

The interaction between the neutral-air wind zonal component and the geomagnetic field will give rise to very different diurnal variations of f_oF_2 at eastward

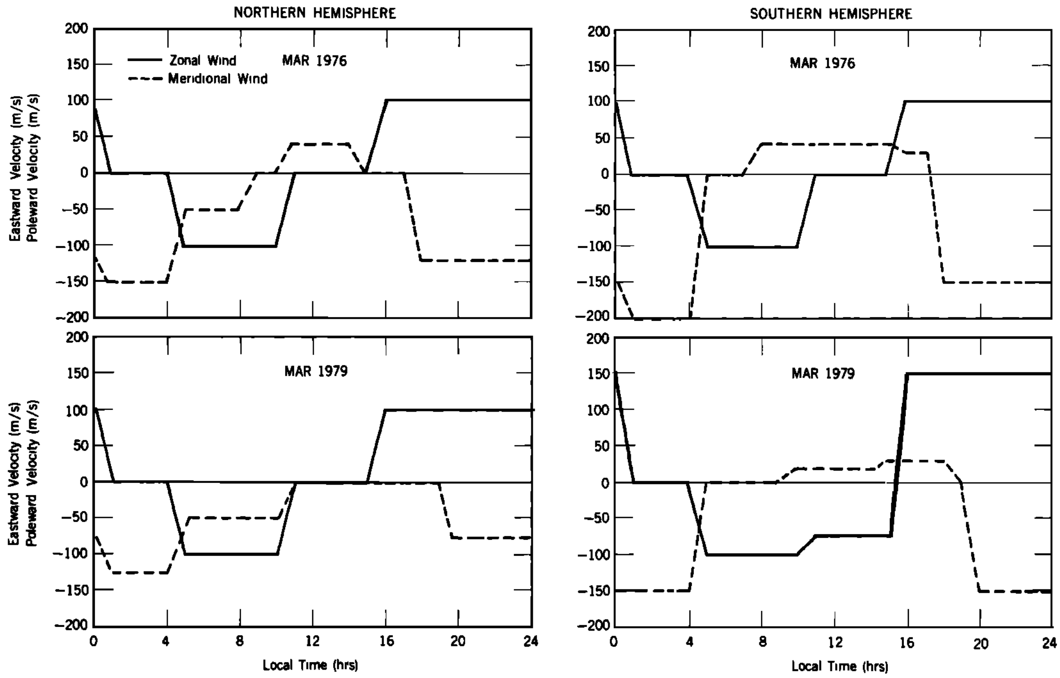

Fig. 2. Meridional and zonal neutral wind models for March 1976 and 1979.

and westward declinations. Simply extrapolating observations from one location to another and taking into account only the magnetic latitude dependence of f_oF_2 could result in placing data in areas where the declination is vastly different. This would give rise to f_oF_2 values in inaccessible regions that are unrealistic and unrepresentative of the area. The magnitude of the error made will depend upon the difference between the declination at the observation location and the extrapolated location.

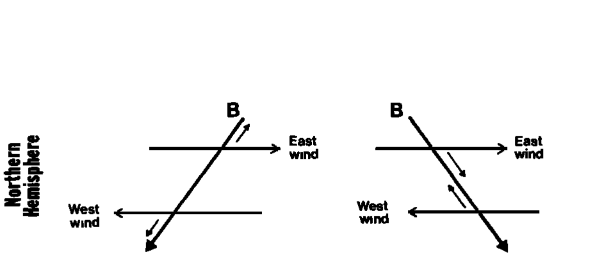

Fig. 3. Geometry illustrating the ionization drift resulting from the interaction of the zonal wind and the magnetic declination. In the figure, $\bar{B}$ is the magnetic field vector, the eastward and westward wind vectors are shown, and the direction of the imparted drift velocity is indicated as a small arrow parallel or antiparallel to $\bar{B}$.

The time-dependent continuity equation was solved numerically by using a Crank-Nicolson [*Crank and Nicolson*, 1947] implicit finite differencing scheme. The two boundaries are at 125 km altitude at the northern and southern ends of the field line. Boundary conditions for the ion density are photochemical equilibrium during the day and 10 ions/cm^3 at night. However, the boundary conditions are not critical, as the appropriate ion densities are reached within a few space steps.

4. RESULTS AND DISCUSSION

The numerical coefficients that represent the global variaton of f_oF_2 which were derived in this study were put into the same format as those of *CCIR* [1982*b*] and *Jones et al.* [1969]. The entire set of coefficients that represent the global variation of f_oF_2 for each month of July 1975 to June 1976 and July 1978 to June 1979 are given by *Rush et al.* [1984]. For each month, a set of coefficients has been derived that is based on observations of f_oF_2 available from the worldwide network of vertical-incidence ionosonde stations. These observations have been supplemented by data obtained from a detailed constant-local-time analysis of $f_o F_2$ observations at low magnetic latitude and by data obtained from the time-dependent continuity equation at the higher latitudes. Typically, for each month, about 20 locations with actual observations and 95 locations of contour-derived $f_o F_2$ values were used for the low-latitude data base. For the higher latitudes for each month, about 75 locations of actual observations and 90 locations of theoretically derived data formed the required data base. If a value of $f_o F_2$ determined from the continuity equation was below 0.7 MHz, the value was set equal to 0.7 MHz. This was done in order to assure that the values of $f_o F_2$ subsequently determined from the numerical coefficients did not yield F_2 region critical frequencies that were near zero or negative.

The accuracy of the coefficients determined from both the diurnal and geographic analysis was computed by use of a least squares method described by *Rush et al.* [1984]. The root-mean-square (rms) error for the fit to the $f_o F_2$ data (observation, contour-derived low-latitude data, and theoretically derived higher-latitude data) for each month for the solar minimum (1975/1976) and solar maximum (1978/1979) time periods is given in Table 3. Also shown in the table is the rms error determined by *Jones et al.* [1969] in deriving the CCIR numerical coefficients for the F_2 region critical frequency. The rms error for the new coefficients is of the order of 0.4–0.5 MHz for the solar minimum representation and between 0.5 and 0.7 MHz for the solar maximum

TABLE 3. RMS Errors (MHz) for the Fit to the Data Used to Generate $f_o F_2$ Coefficients

	New Coefficient		*Jones et al.* [1969]	
Month	Solar Minimum	Solar Maximum	Solar Minimum	Solar Maximum
Jan.	0.513	0.558	0.406	0.662
Feb.	0.375	0.604	0.360	0.607
March	0.428	0.631	0.378	0.619
April	0.425	0.633	0.379	0.600
May	0.310	0.622	0.344	0.585
June	0.334	0.481	0.352	0.583
July	0.337	0.474	0.332	0.581
Aug.	0.392	0.516	0.353	0.553
Sept.	0.449	0.619	0.404	0.589
Oct.	0.452	0.632	0.402	0.650
Nov.	0.400	0.703	0.415	0.699
Dec.	0.379	0.560	0.418	0.696

representation. It can be seen that for the new representation, the rms errors during the solar minimum period are generally one half to two thirds of those at solar maximum. Also, the errors tend to be smaller during the northern hemisphere summer months (May through August) than for the other months of the year.

An example of the global variation of $f_o F_2$ obtained from the coefficients derived in this study is shown in Figure 4. Monthly median contours of $f_o F_2$ (in megahertz) are illustrated for January 1976 at 1200 hours universal time (UT). The figure provides a striking example of the high-latitude trough of ionization typical of the winter nighttime hours (note the contours between 90° and 270° longitude, and poleward of 40° north latitude). Also shown for the late morning and afternoon hours (between 315° and 120° longitude) at latitudes between 30° north and south is the equatorial anomaly. This region is characterized by ionization maxima bounding a relative minimum of ionization above the magnetic equator. The summertime hemisphere, particularly for middle southern hemispheric latitudes, displays values of $f_o F_2$ that vary little with longitude (and local time). This, too, is typical of the F_2 region morphology. The major ionization features depicted on the figure are aligned with magnetic latitude, which explains why, in the geographic representation of the figure, the ionization features tend to be slanted with respect to geographic latitude.

Comparisons between actual observations and $f_o F_2$ derived from the new coefficients and the CCIR coefficients are necessary to determine what, if any, improvement in the global representation of $f_o F_2$ is afforded by the new coefficients. Before discussing improvements, however, it is worthwhile to consider the differences in the values of $f_o F_2$ determined from the two sets of coefficients themselves. Figure 5 shows the diurnal variation of $f_o F_2$ for March 1979 that has been derived from the new coefficients and that derived from the existing CCIR coefficients. Values of $f_o F_2$ are shown for three distinct ranges of declination (eastward, westward, and approximately zero declination) and for five different latitude intervals (northern middle, northern low, equatorial, southern low, and southern middle latitude). The latitudinal intervals are designated according to magnetic latitude. The coordinates of the 15 locations given in the figure are listed in Table 4. For those locations where observations of $f_o F_2$ were available in the generation of the numerical coefficients, the

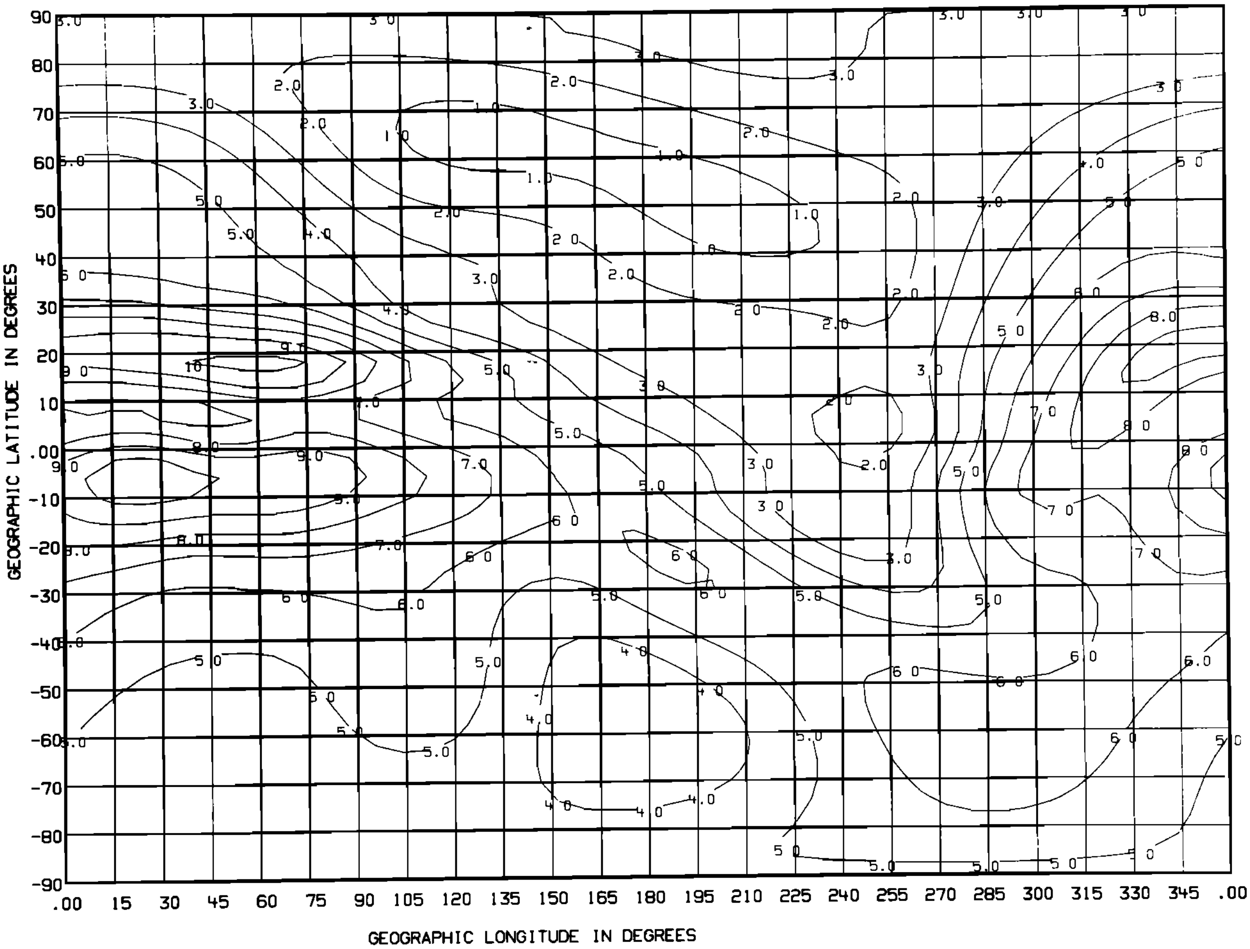

Fig. 4. Contour map of the global representation of the median value of f_oF_2 for January 1976 at 1200 UT derived from the new coefficients.

station indicator begins with a numeral and the station name is listed in Table 4.

The differences between f_oF_2 derived from the two sets of coefficients are rather striking at many of the locations. This is particularly the case for those locations where observations of f_oF_2 were not available (i.e., the locations beginning with a letter). It is at these locations that the biggest differences in the values of f_oF_2 derived from the two sets of coefficients would be expected. The reason for this is that, at unobserved locations, the values of f_oF_2 derived from the numerical coefficients is dependent upon the procedure used to fill in data at the locations in question. As was mentioned earlier, the CCIR coefficients were generated from data that were simply interpolated (or extrapolated) taking account of only the magnetic inclination control of the F_2 region. The new coefficients, on the other hand, were generated from data that accounted for the magnetic inclination and magnetic declination control of the F_2 region.

The results shown in Figure 5 illustrate quite readily the impact of neutral winds on the diurnal variation of f_oF_2 determined from the new coefficients at all locations. This is particularly noticeable for the northern and southern middle-latitude locations. For the 051, 945, and 836 location grouping, the critical frequency during the day hours is highest for the eastward declination and during the night f_oF_2 is highest for the westward declination. The critical fre-

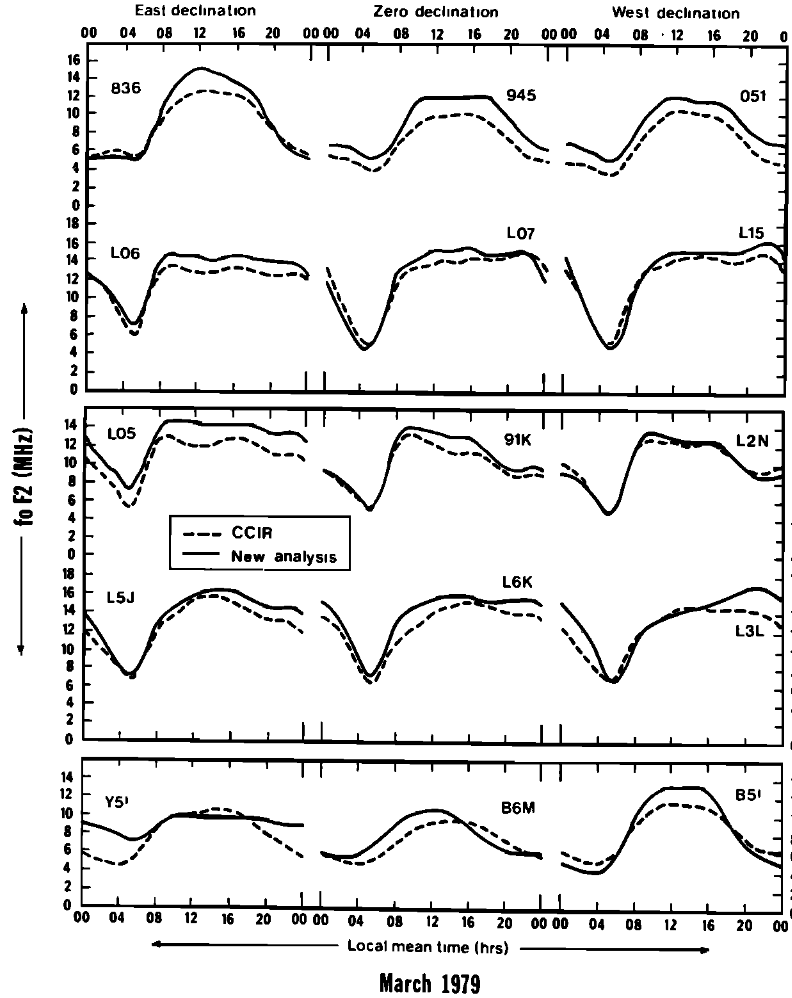

Fig. 5. Diurnal variation of the median value of f_oF_2 during March 1979 determined from the new coefficients and the CCIR coefficients for the northern middle, northern low, equatorial, southern low, and southern middle latitudes at locations with westward, eastward, and zero declinations.

quency for the B5!, B6M, and Y5! location grouping shows exactly the opposite behavior: highest values of f_oF_2 during the day are found at the westward declination and during the night at the eastward declination. This behavior results from the effect of the zonal component of the neutral-air wind on the variation of f_oF_2. It can be seen from Figure 2 that the zonal wind is directed eastward in the evening and westward in the early morning hours in both hemispheres. The zonal wind is directed westward during the day in the southern hemisphere and is zero during the day in the northern hemisphere. In the northern hemisphere, the westward wind during the early morning hours drives ionization up the magnetic field lines where the declination is eastward and down the field lines where the declination is westward (see Figure 3). The ionization that is moved upward is moved into regions of lower loss rates. The values of f_oF_2 are therefore larger at these locations than at locations where the ionization is moved downward into higher loss regions. In the southern hemisphere, recalling Figure 3, the opposite effect is noted. Similar arguments can be made concerning the effect of the zonal wind on f_oF_2 at the other local times.

Figure 5 also provides evidence that neutral-air winds affect the diurnal behavior of the ionization distribution at the low latitudes and even near the equator. For example, f_oF_2 at the northern low-latitude locations during the early morning hours is noticeably lower at the westward declination than at the zero declination location. This agrees with the

TABLE 4. Coordinates of Locations Used to Illustrate Differences in f_oF_2 Derived from the CCIR Coefficients and the New Coefficients

Location Indicator	Geographic Latitude, °N	Geographic Longitude, °E	Magnetic Inclination, °N	Magnetic Declination, °E	Location Name
051	51.5	359.4	66.8	−7.0	Slough
945	45.0	285.0	75.0	0.0	Ottawa
836	35.6	239.4	60.7	15.0	Point Arguello
L15	5.0	310.0	25.1	−16.0	
L07	0.0	290.0	23.9	−2.0	
L06	0.0	240.0	9.9	8.0	
L2N	−10.0	310.0	−6.0	−15.0	
91K	−12.0	285.0	1.0	2.0	Huancayo
L05	0.0	170.0	3.5	10.0	
L3L	−15.0	340.0	−47.2	−22.0	
L6K	−30.0	300.0	−30.3	−2.0	
L5J	−25.0	250.0	−33.6	15.0	
B5!	−49.6	344.4	−57.8	−22.0	
B6M	−64.3	316.5	−58.3	5.0	
Y5!	−50.2	236.2	−62.1	27.0	

expected impact of the zonal wind in the northern hemisphere which is directed westward during the early morning hours. Such effects observed at the low latitudes are particularly encouraging because the data used to supplement the low-latitude observations were not generated using the time-dependent continuity equation. The continuity equation yields values of f_oF_2 that must agree with the effect of neutral-air winds on the ionization distribution. The low-latitude coefficients were generated from data that were either observed or determined from the low-latitude local time analysis. That the resultant values of f_oF_2 agree with theoretical expectation provides further evidence of the validity of the data obtained from the local time analysis.

Figure 6 provides results, similar to those shown in Figure 5, but for the solar minimum period of March 1976. The results displayed in Figure 6 are also in agreement with theoretical expectation. Figure 2 and Figure 3 can be used to verify that this is, indeed, the case.

In order to determine what improvement in f_oF_2 is gained by using numerical coefficients that are consistent with theoretical expectation, differences between observations of f_oF_2 and f_oF_2 deduced from both sets of coefficients (the new coefficients and the CCIR coefficients) must be compared. It is extremely difficult to obtain data that can be used to objectively compare the values of f_oF_2 with observations, particularly in regions of the globe where it is expected that the new coefficients will show the greatest improvement, such as over the oceans. The reasons for this are rather obvious. Any location that is far removed from other locations and for which data were available was used in the generation of the coefficients. To do otherwise would result in coefficients, and hence values of f_oF_2, that could yield needlessly large errors at the very locations where improvement in the specification of f_oF_2 is needed most. One possible approach to overcome this dilemma is to use the numerical coefficients to predict values of f_oF_2 and then to compare the predicted values with observations.

The accuracy of the predicted values of f_oF_2 depends not only on the values of f_oF_2 specified for each month by the coefficients but also on the relationship between solar activity and f_oF_2. The same relationship between f_oF_2 and solar activity was assumed for values determined from both sets of coefficients. This relationship is a linear one between f_oF_2 and the 12-month average sunspot number, R_{12}, given by

$$f_oF_2 = F_l + \left(\frac{F_u - F_l}{R_u - R_l}\right) \cdot R_{12} \qquad (2)$$

where

R_u value of 12-month smoothed sunspot number for solar maximum conditions;

R_l value of 12-month smoothed sunspot number for solar minimum conditions;

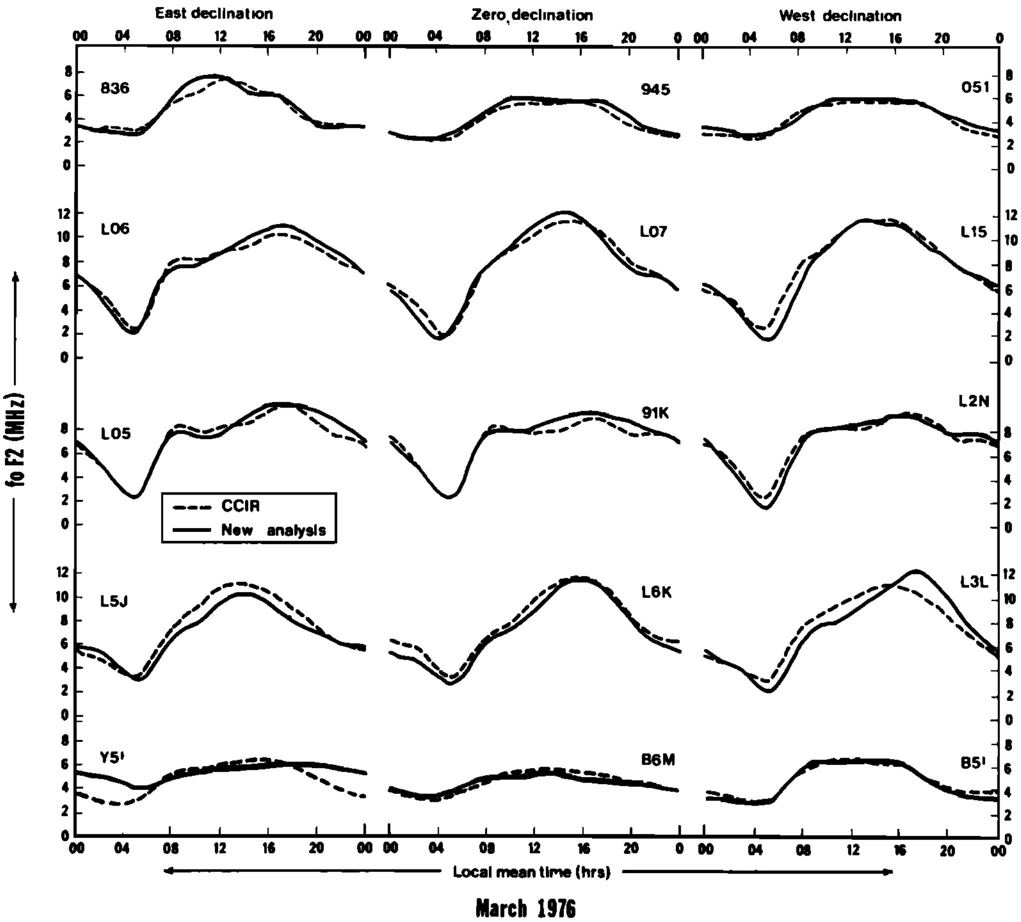

Fig. 6. Diurnal variation of the median value of $f_o F_2$ during March 1976 determined from the new coefficients and the CCIR coefficients for the northern middle, northern low, equatorial, southern low, and southern middle latitudes at locations with westward, eastward, and zero declinations.

F_l value of $f_o F_2$ at R_l;

F_u value of $f_o F_2$ at R_u;

R_{12} value of 12-month smoothed sunspot number for month predictions are being made.

It was further assumed that any errors in $f_o F_2$ resulting from an error in this linear relationship will affect both sets of coefficients equally. The validity of this assumption is questionable, and further study of this is certainly warranted.

Ideally, in order to compare the accuracy of the predictions of $f_o F_2$ by using the new coefficients and by using the current CCIR coefficients, predictions should be made for time periods and for locations that were not used in the development of either set of coefficients. The new coefficients presented here were developed using data observed during, and appropriate to, the solar minimum year of July 1975 through June 1976 and the solar maximum year of July 1978 through June 1979. The CCIR coefficients have been developed by using data valid for the solar minimum period of 1954 through the solar maximum period of 1958. In order to be as objective as possible, comparisons of the prediction accuracy using both sets of coefficients were made for years spanning the early 1960's through 1972.

Table 5 shows the rms prediction errors in $f_o F_2$ determined at Freiburg (48.1°N, 7.6°E) for the months of January, April, July, and October for the years 1964 through 1971. The months January, April, July, and October were chosen because the CCIR has indicated [*CCIR*, 1983] these months as being most representative of the seasonal variations observed in the ionosphere. Data from Freiburg were not used in

TABLE 5. RMS Prediction Errors (MHz) in $f_o F_2$ for Freiburg

	Coefficient Set	Jan.	April	July	Oct.
1964	new	0.54	0.34	0.21	0.32
	CCIR	0.35	0.45	0.23	0.45
1965	new	0.65	0.47	0.23	0.27
	CCIR	0.29	0.64	0.28	0.33
1966	new	0.56	0.39	0.26	0.92
	CCIR	0.40	0.49	0.63	0.41
1967	new	0.42	1.05	0.39	0.49
	CCIR	0.33	1.23	0.48	0.65
1968	new	0.49	0.32	0.67	0.78
	CCIR	0.94	0.31	0.29	0.20
1969	new	0.79	0.52	0.50	0.95
	CCIR	0.60	0.69	0.45	0.32
1970	new	0.52	0.99	0.24	0.45
	CCIR	0.77	1.18	0.68	0.61
1971	new	0.48	0.31	0.27	1.09
	CCIR	0.61	0.41	0.42	0.55

the generation of either set of coefficients. It can be seen that for the months studied, in 20 out of 32 cases, the use of the new coefficients to predict $f_o F_2$ at Freiburg resulted in smaller prediction errors than using the CCIR coefficients. Also worth noting is that the new coefficients tend to have lower prediction errors than the CCIR coefficients during the solar minimum years of 1964, 1965, 1970, and 1971 (13 out of the 16 months) but not during the solar maximum years of 1966, 1967, 1968, and 1969 (7 out of the 16 months).

Comparisons for other locations show that use of the new coefficients does not always lead to improved predictions of $f_o F_2$. Table 6 gives rms prediction errors of $f_o F_2$ by using both the new coefficients and the CCIR coefficients for Grand Bahama, Singapore, Cocos Island, and Hong Kong. Comparisons were made for the same four months as given in Table 5 and for the solar minimum year of 1964 and the solar maximum year of 1969. The prediction errors indicate that the new coefficients do not improve the prediction of $f_o F_2$, particularly during solar maximum conditions (1969). It should be noted, however, that data for three of the four locations given in Table 6—Grand Bahama, Singapore, and Cocos Island—were used in the development of the CCIR coefficients but not in the development of the new coefficients. This may explain, in part at least, the better agreement using the CCIR coefficients.

It is highly likely that the results presented above are colored by errors in the solar activity dependence assumed for the new coefficients in equation (2). The apparent lack of overall improvement in the prediction of $f_o F_2$ using the new coefficients may be due more to deficiency in the solar activity interpolation procedure than to a deficiency in the coefficients themselves. This is based on the fact that for solar minimum conditions the new coefficients tend to yield predicted values of $f_o F_2$ that are either as good as or better than those given by the CCIR coefficients. The solar activity for the months used to determine the new coefficient for solar minimum was, in fact, indicative of minimum solar activity (see Table 1). Thus predictions of $f_o F_2$ at solar minimum are based on coefficients that are realistic representations of solar minimum conditions. The same cannot be said, however, for the new coefficients for solar maximum. The values of the sunspot numbers used to determine the new coefficients varied from 95 in July 1978 to over 150 in June 1979. While values of sunspot numbers of 140–150 are indicative of solar maximum conditions, values of 95–120 may not be. The values of $f_o F_2$ determined from the new coefficients for solar maximum conditions may be too low because they are based on data that may not be totally representative of solar maximum conditions.

The results presented in Table 5 clearly support the above argument. It would be expected that the predictions of $f_o F_2$ for the month of April that are based on the new coefficients would be more accurate than the CCIR coefficients because the data used to derive the new solar maximum coefficients for April were applicable to a sunspot number (140) that

TABLE 6. RMS Prediction Errors (MHz) in $f_o F_2$ at Selected Locations for 1964 and 1969 Solar Activity Conditions

	Year	Coefficient Set	Jan.	April	July	Oct.
Grand Bahama	1964	new	0.90	0.43	0.39	0.53
		CCIR	0.48	0.32	0.30	0.37
Grand Bahama	1969	new	1.40	0.48	0.66	1.05
		CCIR	0.99	0.50	0.41	0.65
Singapore	1964	new	0.53	0.50	0.52	0.51
		CCIR	0.54	0.37	0.45	0.69
Singapore	1969	new	1.31	0.62	1.12	1.19
		CCIR	0.78	0.56	0.48	0.51
Cocos Island	1964	new	0.78	0.94	0.64	0.93
		CCIR	0.75	0.94	0.52	0.65
Cocos Island	1969	new	0.55	1.50	1.31	0.60
		CCIR	0.95	1.78	1.03	0.79
Hong Kong	1969	new	1.53	1.60	1.09	0.93
		CCIR	0.67	1.81	1.16	1.31

is truly representative of solar maximum conditions. Of the results presented for April in Table 5, seven out of eight cases show that f_oF_2 determined from the new coefficients is better than f_oF_2 determined from the CCIR coefficients. Even in Table 6, the results given for the month of April show that the CCIR coefficients do not yield values of f_oF_2 that are vastly better than those determined from the new coefficients. This is particularly noteworthy because, as mentioned previously, observations at Grand Bahama, Singapore, and Cocos Island were used in the generation of the CCIR coefficients but not in the generation of the new coefficients.

The results presented above indicate that the values of f_oF_2 obtained from the new coefficients appear to be better than those obtained from the CCIR coefficients if proper account can be taken of the solar cycle dependence of the coefficients. This result holds true for regions of the globe where observations of f_oF_2 were generally available to determine the numerical coefficients. At locations where data are not available, it is difficult to quantify the improvement afforded by the new coefficients. However, *Rush et al.* [1983] have shown that, for the southern hemisphere, values of f_oF_2 determined from the new coefficients are generally closer to those obtained from the Japanese satellite ISS-b than are the values of f_oF_2 deduced from the CCIR coefficients during December 1978 (a period of solar maximum).

Further validation and verification of the values of f_oF_2 determined from the new coefficients are certainly warranted. This is particularly desirable for regions of the globe that are inaccessible to routine ground-based ionospheric soundings. However, it does appear that the new coefficients afford an opportunity to determine values of f_oF_2 on a global basis that are consistent with observation and with the current physical understanding of the mechanisms that control the F_2 region ionization distribution.

5. CONCLUSIONS

A new set of numerical coefficients to represent the median behavior of the global variation of f_oF_2 has been developed that is consistent with the current understanding of the physical processes that govern the F_2 region. The coefficients enable median values of f_oF_2 to be determined at any location on the globe for any month of the year and for any phase of the solar cycle. The coefficients that have been described in this paper have the same format as those developed by *Jones and Gallet* [1962] which form the basis of many ionospheric propagation prediction methods.

The new coefficients have been determined by using observations of f_oF_2, values of f_oF_2 determined from the time-dependent continuity equation for ions and electrons, and values of f_oF_2 deduced from a constant local-time analysis for the low-latitude F_2 region distribution. The coefficients have been determined for each month of two different years: a year of minimum solar activity (July 1975 to June 1976) and a year near maximum solar activity (July 1978 to June 1979). The time-dependent continuity equation was used to provide values of f_oF_2 in regions of the middle- and high-latitude ionosphere where observations are unavailable. By incorporating realistic models of the F_2 region neutral-air winds into the continuity equations, along with a representation of the geomagnetic field, values of f_oF_2 were determined that include the effect of both the magnetic declination and magnetic inclination control on the F_2 region. A constant local-time analysis was used to determine values of f_oF_2 at low-latitude regions of the globe that are inaccessible to routine ionospheric sounding. It is expected that low-latitude values of f_oF_2 determined from a continuity equation that includes realistic $\bar{\mathbf{E}} \times \bar{\mathbf{B}}$ drifts in the equatorial region would lead to a better representation. Such a study should be pursued.

The new coefficients were used to determine values of f_oF_2 at various locations in the ionosphere for different solar activity conditions. It was found that the new coefficients yielded values of f_oF_2 during solar minimum conditions that were on average better than the values of f_oF_2 determined from the CCIR coefficients. For solar maximum conditions, the results of the analysis carried out in this study indicate that, if adjustments are made to take into account the fact that the data used to generate the solar maximum coefficients are not truly representative of solar maximum conditions for all months, an improved representation of f_oF_2 will emerge. In regions of the globe that are inaccessible to routine observation, the new coefficients yield values of f_oF_2 that differ significantly from those obtained from the CCIR coefficients. The limited validations performed in this study for those inaccessible regions indicate that the new coefficients yield much improved values of f_oF_2. Further validation, using data such as obtained by the ISS-b satellite, is needed before the new coefficients can be recommended as a replacement for the existing CCIR coefficients.

It is necessary that further work be done to improve the solar cycle variation of f_oF_2 determined using the new coefficients. As was indicated in section 4, the values of the new coefficients for periods surrounding solar maximum conditions yield values of f_oF_2 that are not an obvious improvement over the results obtained using the CCIR coefficients. The new coefficients must be adjusted to account for the fact that for some of the months (particularly July through December) in solar maximum, the coefficients were determined from data that may not be truly representative of the maximum solar activity conditions. The relationship chosen to represent the solar cycle variation of f_oF_2 obviously will influence the results obtained for predicted f_oF_2 values. The high prediction errors for both sets of coefficients for some of the months (see Tables 5 and 6) illustrate the fact that equation (2) does not provide realistic predicted values of f_oF_2 for all solar cycle conditions. The method of predicting f_oF_2 described by *Liu and Smith* [1982] may provide a useful approach to improve this situation.

The most promising validation and assessment of the new coefficients may be their use in existing ionospheric models and radio propagation simulation techniques. It has been mentioned many times throughout this paper that the new coefficients have the same format as the current CCIR coefficients. Any ionospheric models or radio propagation prediction techniques using the CCIR coefficients [*CCIR*, 1982*b*] or the coefficients of *Jones et al.* [1969] can readily be adapted to using the new coefficients. Results of ionospheric modeling efforts and radio propagation simulation studies obtained by using both the CCIR coefficients and the new coefficients would prove to be invaluable in the final assessment of the improvement afforded by the new coefficients.

Acknowledgments. Throughout the course of this study the authors benefited greatly from discussions with Kenneth Davies, NOAA/SEL. Douglass Crombie, Chief Scientist, NTIA, provided valuable comments concerning the presentation of results, as did Edgar Hayden, Southwest Research Institute.

REFERENCES

Anderson, D. N., A theoretical study of the ionosphere *F* region equatorial anomaly, I, Theory, *Planet. Space Sci.*, *21*, 409–419, 1973.

Barghausen, A. F., J. W. Finney, L. L. Proctor, and L. D. Schultz, Predicting long-term operational parameters of high frequency sky-wave telecommunications systems, *Rep. N70-24144*, Natl. Tech. Info. Serv., Springfield, Va., 1969.

Benkhe, R., and H. Kohl, The effects of neutral winds and electric fields on the ionospheric *F*2-layer above Arecibo, *J. Atmos. Terr. Phys.*, *36*, 325–333, 1974.

Bent, R. B., J. R. Lepofsky, S. K. Llewellyn, and P. G. Schmid, Ionospheric range-rate effects in satellite-to-satellite tracking, Operational Modelling of the Aerospace Propagation Environment, vol. I, edited by H. Soicher, *AGARD Conf. Proc.*, *230*, 9-1–9-15, 1978.

CCIR, Supplement to report 252-2, Second CCIR computer-based interim method for estimating sky-wave field strength and transmission loss at frequencies between 2 and 30 MHz, in *Recommendations and Reports of the CCIR, 1982*, vol. VI, Geneva, 1982*a*.

CCIR, Report 340-4, CCIR atlas of ionospheric characteristics, in *Recommendations and Reports of the CCIR*, vol. VI, Geneva, 1982*b*.

CCIR, Report of interim working parties 6/12 and 10/5 to study group 6 and 10, Geneva, 1983.

Crank, J., and P. Nicolson, A practical method for numerical evaluation of solutions of partial differential equations of the heat-conductor type, *Math Proc. Cambridge Philos. Soc.*, *43*, 50–67, 1947.

Crow, E. L., and D. H. Zacharisen, The error in prediction of *F*2 maximum usable frequencies by world maps based on sunspot number, in *Proceedings of Symposium on Statistical Methods in Radio Wave Propagation, Univeristy of California, Los Angeles*, edited by W. C. Hoffman, Symposium Publications Division, Pergamon, New York, 1960.

Haydon, G. W., M. Leftin, and R. K. Rosich, Predicting the performance of high frequency skywave telecommunication systems, *Rep. PB258566/AS* Natl. Tech. Info. Service, Springfield, Va., 1976.

Jones, W. B., and R. M. Gallet, The representation of diurnal and geographic variations of ionospheric data by numerical methods, *Telecommun. J.*, *29*, 129–149, 1962.

Jones, W. B., and R. M. Gallet, Representation of diurnal and geographic variations of ionospheric data by numerical methods, *Telecommun. J.*, *32*, 18–28, 1965.

Jones, W. B., R. P. Graham, and M. Leftin, Advances in ionospheric mapping by numerical methods, *ESSA Tech. Rep. ERL 107-ITS 75*, Environ. Res. Lab., Boulder, Colo., 1969.

King, J. W., and A. J. Slater, Errors in predicted values of f_oF_2 and h_mF_2 compared with the observed day-to-day variability, *Telecommun. J.*, *40*, 766, 1973.

Liu, R. Y., and P. A. Smith, A new method of predicting *F*2-layer critical frequencies, *Telecommun. J.*, *49*, 416–420, 1982.

Lucas, D. L., and G. W. Haydon, Predicting statistical performance indexes for high frequency telecommunications systems, *Rep. AD644-827*, Natl. Tech. Info. Serv., Springfield, Va., 1966.

Nielson, D. L., J. B. Lomax, and H. A. Turner, The prediction of nuclear effects on HF communication, *Proj. Rep. 5481*, Stanford Res. Inst., Menlo Park, Calif., November 1967.

Nisbet, J. S., On the construction and use of a simple ionospheric model, *Radio Sci.*, *6*, 437–464, 1971.

Rush, C. M., M. PoKempner, D. N. Anderson, and F. G. Stewart, The use of theoretical models to improve global maps of f_oF_2, *Rep. PB82-187170*, Natl. Tech. Info. Serv., Springfield, Va., 1982.

Rush, C. M., M. PoKempner, D. N. Anderson, F. G. Stewart, and J. Perry, Improving ionospheric maps using theoretically derived values of f_oF_2, *Radio Sci.*, *18*, 95–107, 1983.

Rush, C. M., M. PoKempner, D. N. Anderson, J. Perry, F. G.

Stewart, and R. Reasoner, Global maps of $f_o F_2$ derived from observations and theoretical values, *Rep. PB84-163906*, Natl. Tech. Info. Serv., Springfield, Va., 1984.

Teters, L. R., J. L. Lloyd, G. W. Haydon, and D. L. Lucas, Estimating the performance of telecommunication systems using the ionospheric transmission channel—Ionospheric communications analysis and prediction program user's manual, *Rep. PB84-111210*, Natl. Tech. Info. Serv., Springfield, Va., 1983.

D. N. Anderson, Air Force Geophysics Laboratory, Hanscom Air Force Base, MA 01731.

J. Perry, Department of Defense, Washington, D. C. 20755.

M. PoKempner, R. Reasoner, C. M. Rush, and F. G. Stewart, Institute for Telecommunication Sciences, National Telecommunications and Information Administration, U.S. Department of Commerce, Boulder, CO 80303.